SUPPLEMENTAL MATERIAL

Karmaus et al., https://doi.org/10.1084/jem.20161855

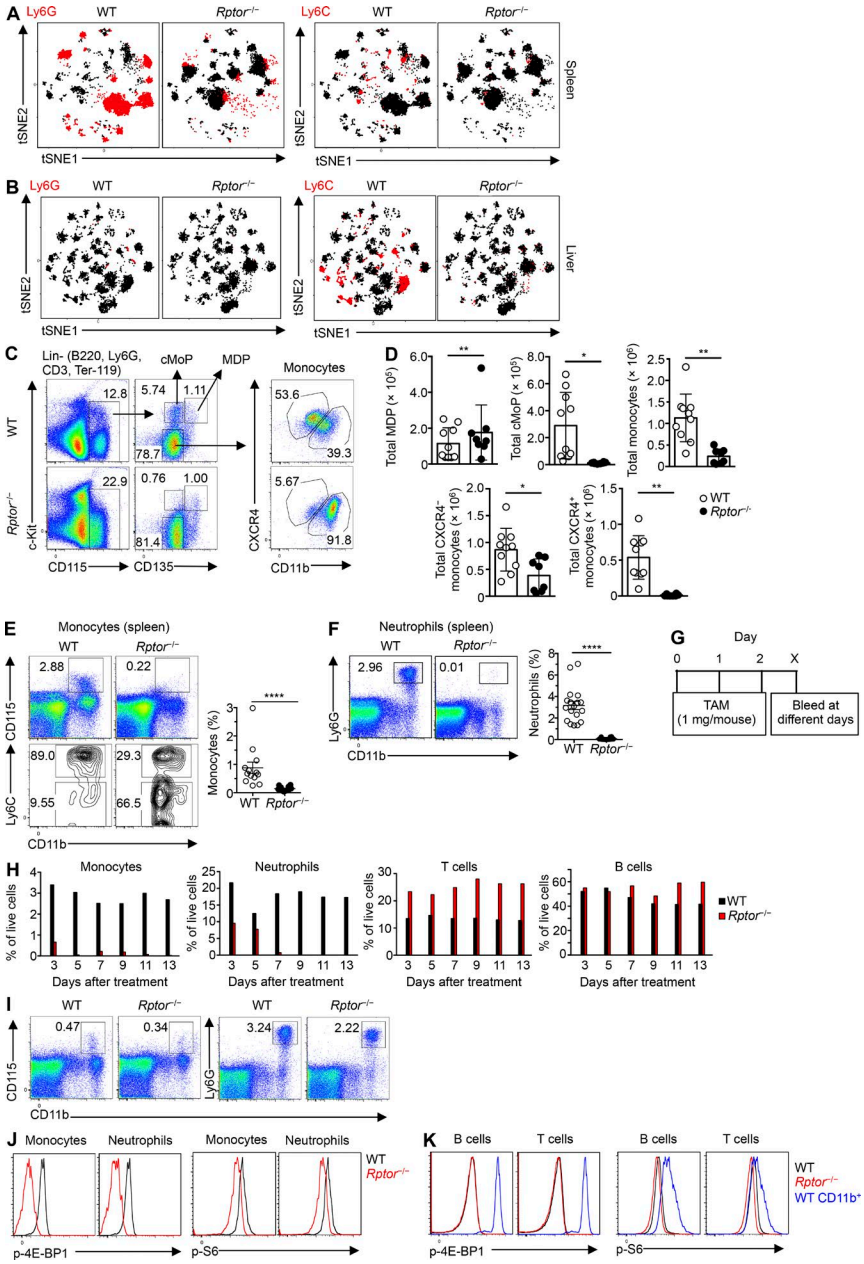

Figure S1. **Raptor ablation causes homeostatic loss of monocytes, macrophages, and neutrophils.** (A) tSNE dimensionality reduction of flow cytometry data of gated CD11b$^+$ cells from the spleen of WT and *Rptor*$^{-/-}$ mice. Positive staining levels of Ly6G and Ly6C are colored in red (n = 4–5 mice per group). (B) tSNE dimensionality reduction of flow cytometry data of gated CD11b$^+$ cells from the liver of WT and *Rptor*$^{-/-}$ mice. Positive staining levels of Ly6G and Ly6C are colored in red (n = 4–5 mice per group). (C) Gating strategy for cMoP, MDP, and monocytes in BM cells of WT and *Rptor*$^{-/-}$ mice. (D) Numbers of monocyte precursor populations in BM of WT and *Rptor*$^{-/-}$ mice after *L. monocytogenes* infection according to the gating depicted in S1C (n = 4–5 mice per group). (E) Flow cytometry analysis (top left) and frequency (right) of monocytes (CD11b$^+$CD115$^+$) in spleen of WT and *Rptor*$^{-/-}$ mice. Flow cytometry analysis (bottom left) of classic (Ly6C^{hi}) and nonclassic (Ly6C^{lo}) monocytes (gated on CD11b$^+$CD115$^+$ monocytes) in spleen of WT and *Rptor*$^{-/-}$ mice. (F) Flow cytometry analysis (left) and frequency (right) of neutrophils (CD11b$^+$Ly6G$^+$) in spleen of WT and *Rptor*$^{-/-}$ mice. (G) Scheme of experimental design of tamoxifen treatment and continuous bleeding. (H) Cell percentages of blood monocytes, neutrophils, T cells, and B cells from WT and *Rptor*$^{-/-}$ mice. (I) Flow cytometry analysis of monocytes (CD11b$^+$CD115$^+$; left) and neutrophils (CD11b$^+$Ly6G$^+$; right) in spleen of WT and *Rptor*$^{-/-}$ mice at 4 d after the initial injection of tamoxifen. (J) Flow cytometry analysis of phosphorylation of 4E-BP1 (left) and S6 (right) in monocytes and neutrophils in spleen of WT and *Rptor*$^{-/-}$ mice. (K) Flow cytometry analysis of phosphorylation of 4E-BP1 (left) and S6 (right) in B cells and T cells from the spleen of WT and *Rptor*$^{-/-}$ mice (levels in WT CD11b$^+$ cells are shown in comparison). Numbers indicate percentage of cells in gates. Data are mean ± SEM. Data are representative of four (A and B), six (C and D), 14 (E and F), or two (G–K) independent experiments. *, P < 0.05; **, P < 0.01; ****, P < 0.0001; Student's t test for parametric data or Mann–Whitney test for nonparametric data.

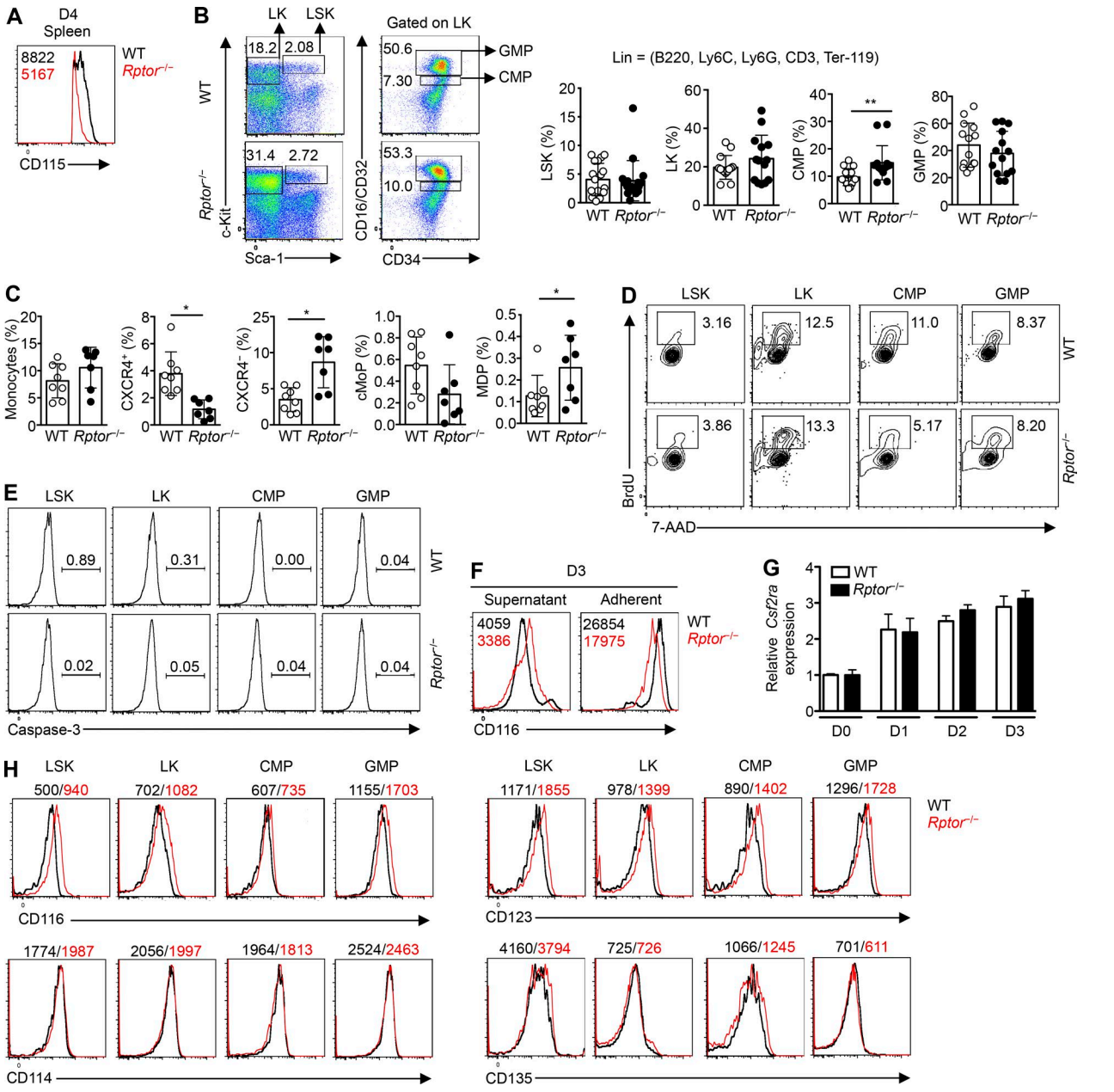

Figure S2. **Loss of Raptor has limited effects on precursor composition and cytokine receptor expression aside from M-CSFR.** (A) Expression of CD115 on CD11b^{+}CD115^{+} monocytes in the spleen of WT and *Rptor*$^{-/-}$ mice at day 4 after tamoxifen treatment, with mean fluorescence intensity (MFI) plotted within graph. (B) Gating strategy for LSK and LK by c-Kit and Sca-1 within Lin^{-} cells (left), and CMP and GMP within LK population (right) in BM cells of WT and *Rptor*$^{-/-}$ mice. Right, frequencies of indicated cell populations. (C) Frequencies of total and CXCR4^{+} or CXCR4^{-} monocytes and cMoP and MDP in BM cells from WT and *Rptor*$^{-/-}$ mice. (D) Flow cytometry analysis of BrdU and 7-AAD in WT and *Rptor*$^{-/-}$ myeloid progenitor cell populations. (E) Flow cytometry analysis of active caspase-3 in WT and *Rptor*$^{-/-}$ myeloid progenitor cell populations. (F) Expression of CD116 on supernatant and adherent cell fractions of WT and *Rptor*$^{-/-}$ Lin^{-} BM cells after liquid culture with M-CSF (10 ng/ml) for 3 d, with MFI plotted within graphs. (G) Analysis of *Csf2ra* mRNA in WT and *Rptor*$^{-/-}$ Lin^{-} cells after liquid culture with M-CSF (10 ng/ml) for 0, 1, 2, or 3 d. (H) Expression of CD116, CD114, CD123, or CD135 on WT and *Rptor*$^{-/-}$ Lin^{-} BM myeloid progenitor populations, with MFI plotted above graphs. Numbers indicate percentage of cells in gates. Data are mean ± SEM and representative of two (A and C–E), 14 (B), four (F and G), or five (H) independent experiments. *, $P < 0.05$; **, $P < 0.01$; Mann–Whitney test.

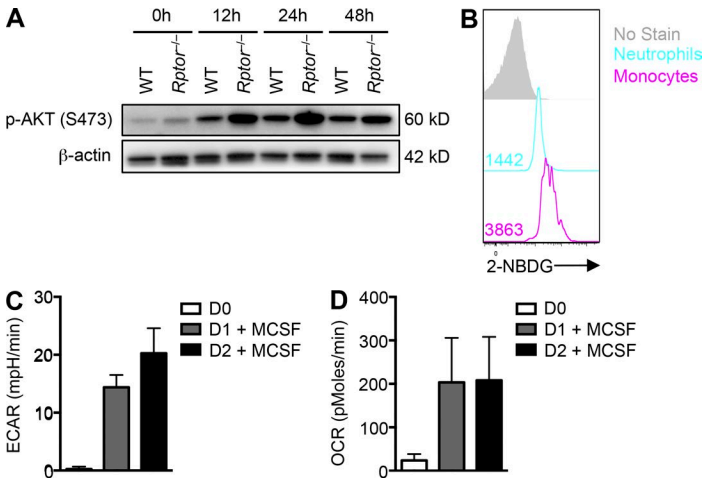

Figure S3. **High glucose uptake and M-CSF–induced metabolic activation in myeloid cells.** (A) Immunoblot analysis of phosphorylated AKT and β-actin in fresh (0 h) or M-CSF–stimulated (10 ng/ml, for the indicated times) Lin⁻ cells from WT and *Rptor*$^{-/-}$ mice. (B) 2-NBDG staining of neutrophils and monocytes in spleen of WT mice, with mean fluorescence intensity (MFI) plotted within graph. (C) Measurement of ECAR in freshly isolated Lin⁻ cells or those stimulated with M-CSF (10 ng/ml) for 1 or 2 d. (D) Measurement of OCR in freshly isolated Lin⁻ cells or those stimulated with M-CSF (10 ng/ml) for 1 or 2 d. Data are representative of two (A, C, and D) or three (B) independent experiments.

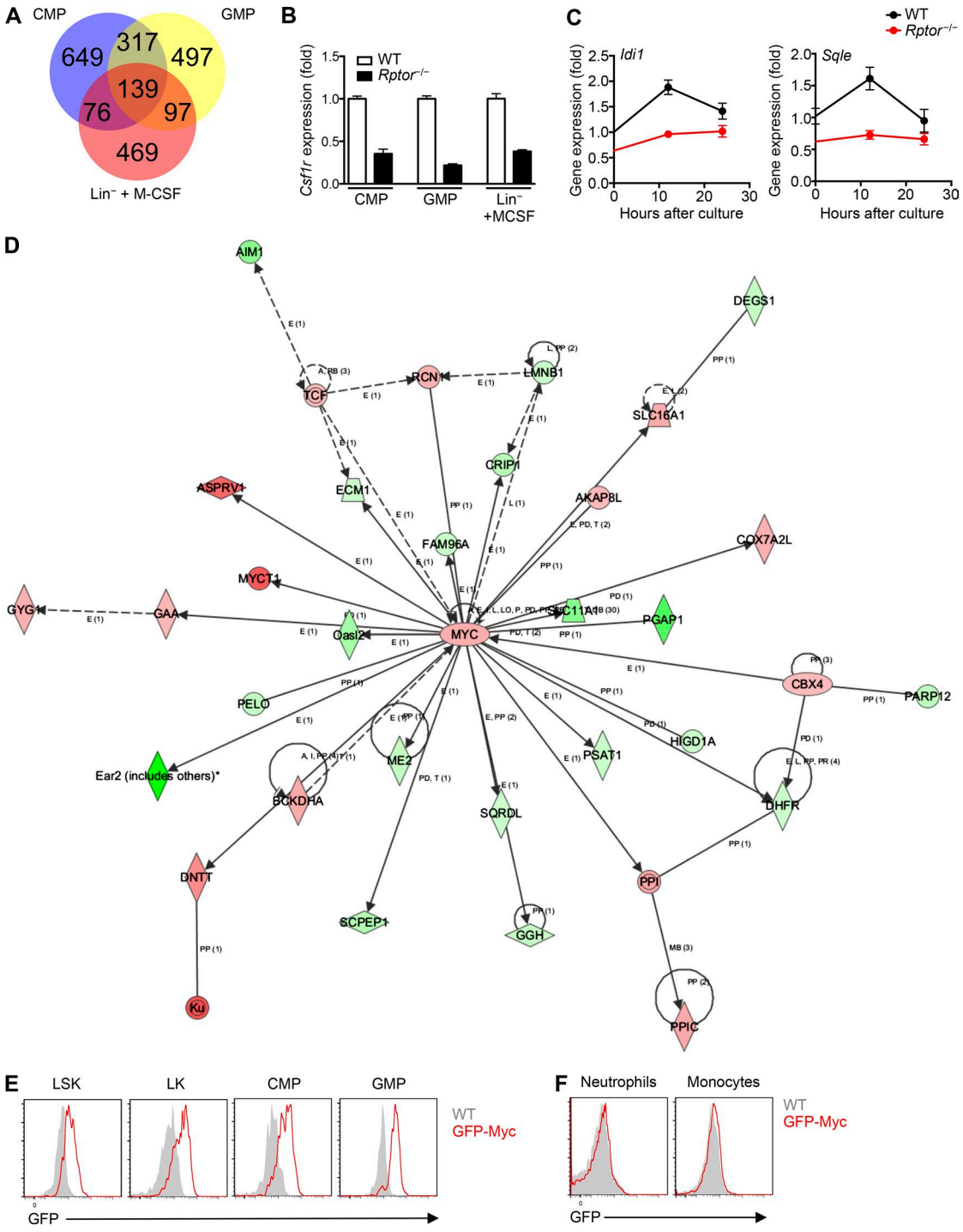

Figure S4. **Myc is expressed in myeloid precursors, but not in mature myeloid cells.** (A) Summary of differentially expressed genes between WT and *Rptor*$^{-/-}$ cells in CMP, GMP, and M-CSF–stimulated Lin$^-$ cells (CMP and GMP: $n = 3$ mice per group; Lin$^-$ + M-CSF: $n = 4$ mice per group). (B) Relative *Csf1r* expression of WT and *Rptor*$^{-/-}$ CMP, GMP, and M-CSF–stimulated Lin$^-$ cells (CMP and GMP: $n = 3$ mice per group; Lin$^-$ + M-CSF: $n = 4$ mice per group). (C) Relative gene expression of *Idi1* and *Sqle* in WT and *Rptor*$^{-/-}$ Lin$^-$ cells stimulated with M-CSF (10 ng/ml) for 0, 12, or 24 h. (D) Top differentially regulated gene network (energy production, molecular transport, carbohydrate metabolism) between *Rptor*$^{-/-}$ and WT cells in transcriptome profiling, showing Myc as a central node ($n = 4$ mice per group). (E) Expression of GFP-Myc in myeloid progenitor cell populations from WT and GFP-Myc mice. (F) Expression of GFP-Myc in mature myeloid cells from WT and GFP-Myc mice. Data are one experiment (A, B, and D) or representative of two independent experiments (C, E, and F).

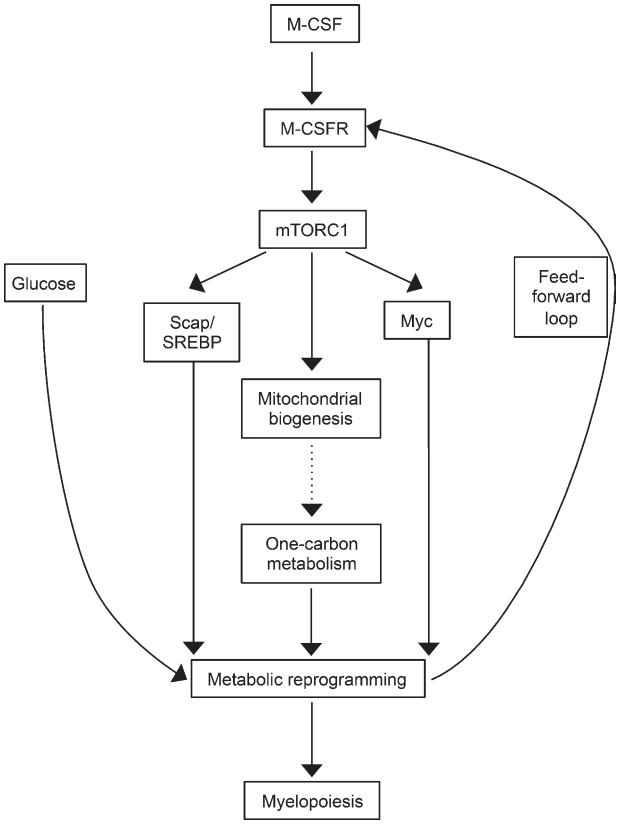

Figure S5. **Model of mTORC1–mediated metabolic reprogramming and feed–forward loop in M-CSF–dependent myelopoiesis.** M-CSF drives the activation of mTORC1 via M-CSFR signaling. mTORC1 links this signal to metabolic pathways including Scap/SREBP, Myc, and mitochondrial biogenesis, which supports one-carbon metabolism. Together, these pathways reprogram the metabolism of myeloid precursor cells during myelopoiesis. This process requires glucose as a carbon source, which, together with M-CSF, participates in a feed-forward loop to drive myelopoiesis. Overall, this model depicts a metabolism-centric view of M-CSF–dependent myelopoiesis. For clarity, myeloid-specific transcription factors are not included.